

Supercritical Fluid-Assisted Fabrication of Pd Nanoparticles/Graphene Using a Choline Chloride–Oxalic Acid Deep Eutectic Solvent for Enhancing the Electrochemical Oxidation of Glycerol

Cheng-Hao Liao, Jing-Ying Chen, Guang-Yang Liu, Zhe-Rui Xu, Sheng Lee, Cheng-Kang Chiang,* and Yi-Ting Hsieh*



Cite This: *ACS Omega* 2022, 7, 19930–19938

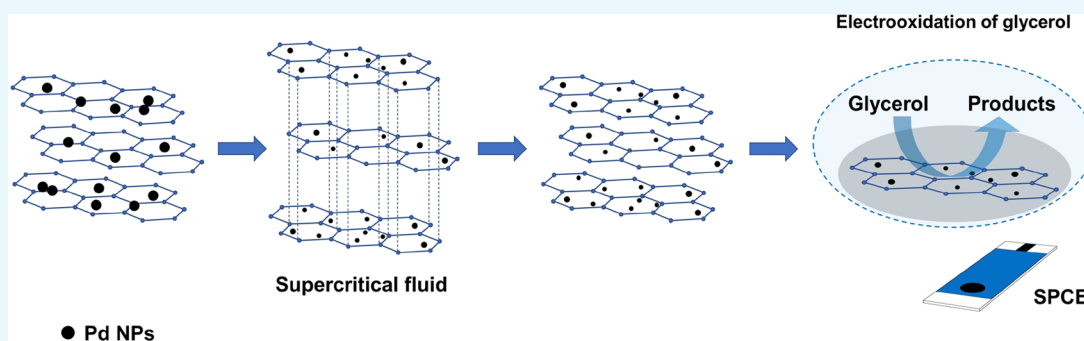


Read Online

ACCESS |

Metrics & More

Article Recommendations



ABSTRACT: A green method for synthesizing Pd nanoparticles/graphene composites from a choline chloride–oxalic acid deep eutectic solvent (DES) without a reducing agent or a surfactant is reported. Deep eutectic solvents are usually composed of halide salts and hydrogen-bond donors, and many are biocompatible and biodegradable. The merits of deep eutectic solvents include that they serve as reducing agents and dispersants, and Pd nanoparticles are tightly anchored to graphene. The size and dispersion of Pd particles are improved when supercritical carbon dioxide (scCO₂) is used because it has gaslike diffusivity and near-zero surface tension, which results in excellent wettability between the scCO₂ and the carbon surface. The prepared sc-Pd NPs/GR/SPCE shows excellent activity toward glycerol oxidation compared to composites not fabricated by scCO₂ processes. This study demonstrates the potential of using this scCO₂-assisted protocol combined with deep eutectic solvents to further construct nanoparticles/graphene composites.

INTRODUCTION

Because of their fascinating size- and shape-dependent properties, metal nanoparticles have attracted great interest in the fields of catalysis and sensing for decades. Achieving environmentally friendly and sustainable methods for preparing such nanomaterials is now a worldwide demand. In today's world, the environmental impact of solvents, reductants, and stabilizing agents used in preparing nanoparticles needs to be considered.

Most deep eutectic solvents (DESs) are mixtures composed of quaternary ammonium salts and hydrogen-bond donors (HBD) such as sugars, alcohols, and the amino acid, at specific ratios. The mixture has a lower melting point than either of its components. DESs have been used in synthesis, separation, industry, and electrochemistry, becoming an alternative to traditional ionic liquids. DESs offer many advantages over ionic liquids, including biodegradability, biocompatibility, simpler synthesis, and low cost.^{1–4} DESs have been increasingly applied for advancing the low-temperature synthesis, function-

alization, and application of nanomaterials. DESs have been used to functionalize carbon and metal-based nanomaterials and size- and shape-controlled synthesis of metal nanomaterials.^{1,5–7} Sun and co-workers reported that DESs are versatile systems and can be used in the electrochemical shape-controlled synthesis of high-index faceted nanocrystals, including Pt concave THH enclosed by {910} facets and Au TOH with a {311} facet. The adsorbed ions of DESs such as choline cations, Cl[−], and urea served as regulators of surface structure. Moreover, they also reported that the urea HBD preferentially stabilizes the (100) faces of Pt seeds and blocks the growth of the <100> axis.^{8–10} Only a few reports have

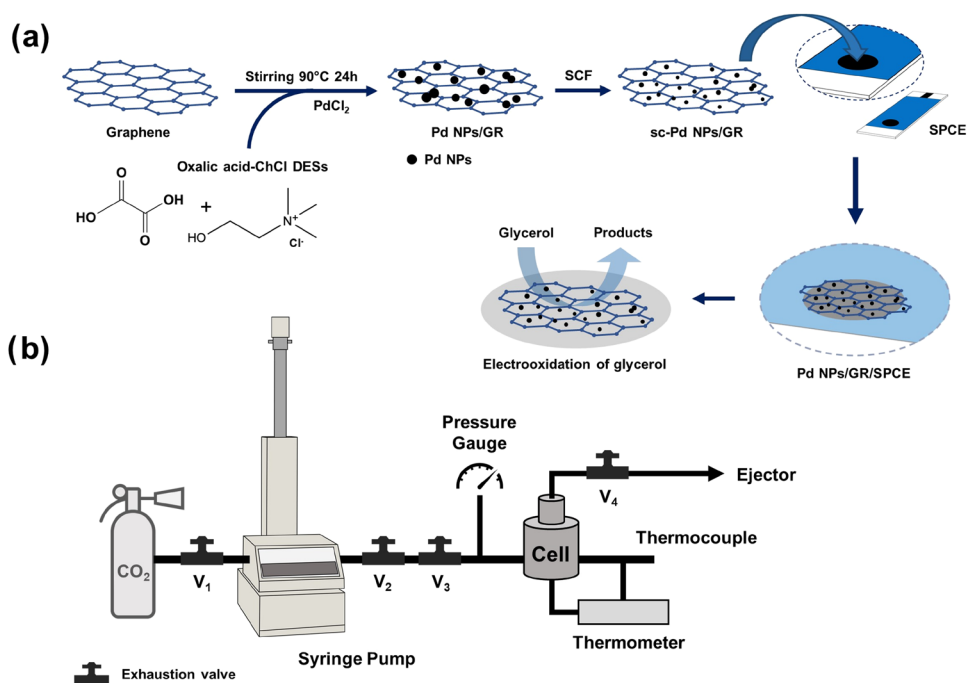
Received: March 22, 2022

Accepted: May 19, 2022

Published: June 2, 2022



Scheme 1. (a) Fabrication of (sc)-Pd NPs/GR-Modified Electrode and the Application of Glycerol Catalysis. (b) Instrumental Setup of the Supercritical CO₂ System



appeared regarding DESs as promising solvents, dispersants, and shape-controlled agents in synthesizing various nanomaterials.^{9,11,12} Liao and co-workers reported that star-shaped Au NPs could be reduced by *L*-ascorbic acid in a ChCl-urea DES.⁹ Oh et al.¹² used a ChCl-malonic acid DES as the reaction medium and a structure-directing reagent to synthesize highly monodispersed gold microparticles. However, in both studies, an additional reducing agent, such as ascorbic acid, was needed to reduce the Au NPs. Chen et al. reported that the ChCl-thiourea DES could act as a solvent, structure-controlling reagent, and offered an in situ sulfur source to synthesize FeS by the ionothermal method.¹¹ To date, only a limited number of in-depth studies have appeared regarding DESs as reducing agents for nanoparticle synthesis. Thus, ChCl-oxalic acid DES was chosen as a solvent and a reducing agent to prepare the nanomaterials in this study. Compared to a traditional organic solvent, a supercritical fluid (SCF) is an attractive alternative for nanoparticle synthesis because such solvents are usually nontoxic, nonflammable, inexpensive, and easily separated.^{13,14} The size and structures of nanoparticles can be readily controlled by utilizing the unique properties associated with such solvents in their supercritical state. When the substance reaches the supercritical state, the properties such as density, dielectric constant, and solubilizing capacity are drastically changed. The properties of a substance in the supercritical state can be adjusted through changes in temperature and pressure. The system can be easily tuned to the optimal setpoint for producing the desired nanoparticle features.¹⁵ Supercritical carbon dioxide (scCO₂) is the most commonly used solvent because it is environmentally friendly, nonflammable, chemically inert, and relatively inexpensive. Moreover, many organometallic precursors with long alkyl chains that cannot typically be utilized in supercritical water (scH₂O) or supercritical ethanol (scEtOH) can be solubilized in scCO₂ because the scCO₂ has a similar density to the liquid carbon dioxide, which retains equal solvation power.^{13,16–19} Pd

nanomaterials have proven to be excellent catalysts in many reactions, including organic coupling reactions, fuel cells, hydrogen storage, and sensing. Owing to the wide range of applications of this element, many techniques for the synthesis of Pd nanostructures have been developed, including deposition using a supercritical fluid. Some examples showing the range of Pd nanomaterials prepared in scCO₂ have appeared.^{18–23} To prepare versatile Pd nanomaterials, the size of the Pd nanoparticles (NPs) is usually reduced, and they are supported on various carbon materials.^{24,25} Graphene (GR) with excellent electrical conductivity and a high surface area represents an excellent support material and, when used, it improves the electronic properties of nanomaterials through the strong interactions between the graphene and the Pd nanoparticles.^{16,21} Therefore, Pd NPs/GR composites are potential materials for use in electrochemical sensors and as catalysts. Polyols such as ethylene glycol and glycerol have several advantages over the traditional fuels (methanol, ethanol, and formic acid) used for energy conversion in fuel cells. These include lower prices, high theoretical energy density, and less toxicity. However, only glycerol is a product that is derived from biomass because it is a natural product that is produced in the methanolysis of vegetable oils. These characteristics make it an excellent candidate for use in fuel cells. The use of glycerol in direct glycerol fuel cells has been widely reported as a prospective energy source for many applications.^{26–31}

This work reports the successful synthesis of Pd NPs/GR composites from a choline chloride–oxalic acid deep eutectic solvent without needing a reducing agent or a surfactant. This method takes advantage of DESs that simultaneously serve as the reducing agent, a particle stabilizer, and the actual reaction media. The size and the distribution of Pd NPs on graphene are highly dependent on the SCF used for the synthesis. The (sc)-Pd NPs/GR/SPCEs were used to electro-oxidize glycerol in an alkaline solution for potential use in direct alcohol fuel

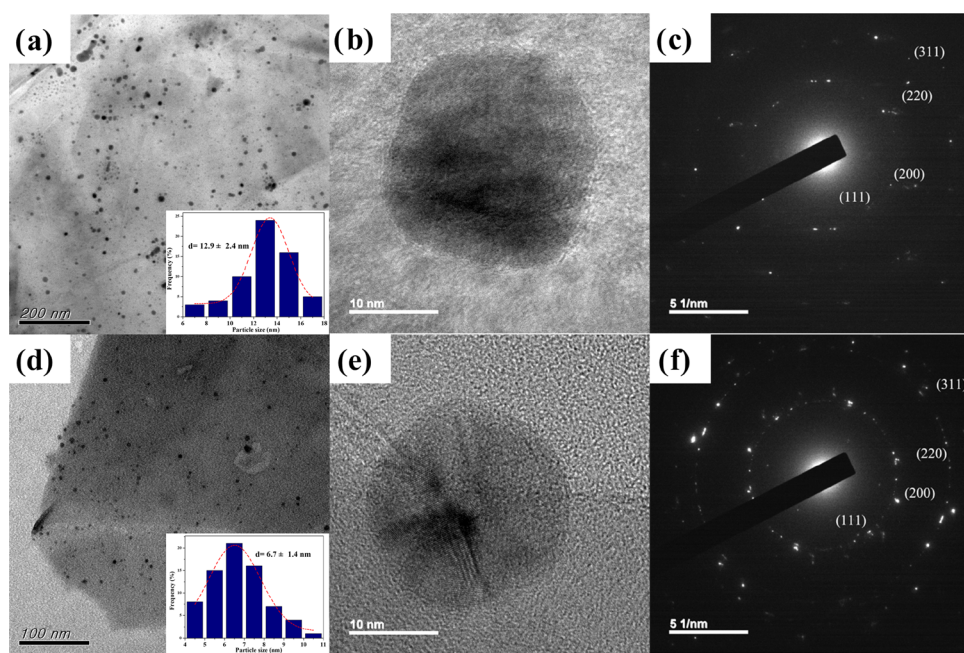


Figure 1. TEM images (a, b, d, e) and SAED patterns (c, f) of Pd NPs/GR (a–c) and sc-Pd NPs/GR (d–f). Inset: size distribution histograms.

cell applications. The schematic illustration (sc-) Pd NPs/GR/SPCE preparation process is shown in Scheme 1a.

EXPERIMENTAL SECTION

Chemicals and Materials. Choline chloride (ChCl, Alfa Aesar, $\geq 99\%$), oxalic acid (Alfa Aesar, 98%), palladium(II) chloride (PdCl_2 , UniRegion Bio-Tech, 99.9%), potassium hydroxide (KOH, Merck, 85%), glycerol (RD, ACS), potassium hexacyanoferrate(III) ($\text{K}_3[\text{Fe}(\text{CN})_6]$, Showa Chemical Co., Ltd, 98%), potassium chloride (KCl, Showa, 99%), and multilayer graphene (Energe, Inc, P-ML20) are used as received. Deionized water (DI water) with a resistivity of 18.2 $\text{M}\Omega$ was prepared using a Merck Water System, and this was used in all experiments.

Preparation of the Pd nanoparticles/graphene composite: The ChCl-oxalic acid deep eutectic solvent (DES) was prepared from a mixture of ChCl and oxalic acid in a 1:2 molar ratio. The mixture was heated and stirred in a beaker at 90 °C for 24 h. Briefly, 20 g of ChCl-oxalic acid DES was added to a 100 mL round-bottom flask, and then 0.015 g of graphene and 0.086 g of PdCl_2 were injected into the round-bottom flask in an oil bath and heated to 90 °C for 24 h under magnetic stirring. The final product had a black color. The products were collected by centrifugation (15 000 rpm) and washed with ethanol five times. Finally, the Pd nanoparticles/graphene (Pd NPs/GR) composites were dispersed into ethanol to produce a colloidal solution for further use.

Supercritical CO_2 Treatment of Pd NPs/GR. Pd NPs/GR (15 mg) was placed in a 25 mL beaker and transferred into a 10 mL stainless steel high-pressure cell (cell, Scheme 1b). The system was first purged with CO_2 and maintained at 50 °C. After closing valve 4, the system was pressurized with 10.3 MPa of CO_2 for the supercritical CO_2 treatment step. After a 5 min incubation, the system was depressurized by opening valve 4 to release CO_2 . The Pd nanoparticles/graphene composites (sc-Pd NPs/GR) were collected and purified by centrifugation at 12 500 rpm for 5 min and washed five times with ethanol.

Finally, the as-prepared sc-Pd NPs/GR was dispersed into ethanol for further use.

Characterization. The morphology and the composition of the (sc-) Pd NPs/GR were observed by transmission electron microscopy (TEM) and high-resolution TEM. X-ray diffraction (XRD) patterns were recorded with a Bruker D2 PHASER instrument with a $\text{Cu K}\alpha$ radiation source; scanning was conducted over 35–80° (2θ). An inductively coupled plasma optical emission spectrometer (ICP-OES, Agilent 725) was used to detect Pd. The surface compositions were evaluated with an XPS photometer (Thermo, K- α) using a $\text{Mg K}\alpha$ radiation source (12 kV and 10 mA). The binding energy scale was calibrated to 284.3 eV based on the prominent C 1s peak.

Electrochemical Measurement. All electrochemical studies were conducted on a Metrohm Autolab PGSTAT 204 potentiostat/galvanostat controlled by NOVA software. A standard three-electrode electrochemical setup was employed in all experiments. A spiral Pt wire was used as the counter electrode, and a Ag/AgCl electrode was used as the reference electrode. A screen-printed carbon electrode (SPCE, 0.018 cm^2 , SE102, Zensor) was cleaned by treatment with deionized (DI) water and then activated by cyclic voltammetry in a 0.1 M phosphate buffer solution (pH 7) at room temperature for 10 cycles. For preparing the Pd NPs/GR/SPCE, 2.0 mg of Pd NPs/GR powder was dispersed in 0.1 mL of ethanol by ultrasonic agitation to give a homogeneous suspension. Finally, 1.0 μL of 20 mg mL^{-1} suspension solution was drop-cast on the activated SPCE surface and dried under an infrared lamp (175 W) for 10 min. All cyclic voltammetry experiments for the electro-oxidation of glycerol were operated at potentials ranging from -0.6 to $+0.6$ V in both 1 M KOH and 1 M glycerol/1 M KOH solutions. To evaluate the stability of the material, chronoamperometry (CA) for glycerol oxidation was measured at the -0.1 V (vs Ag/AgCl) for an hour for both (sc-) Pd NPs/GR/SPCE in a 1 M glycerol/1 M KOH solution.

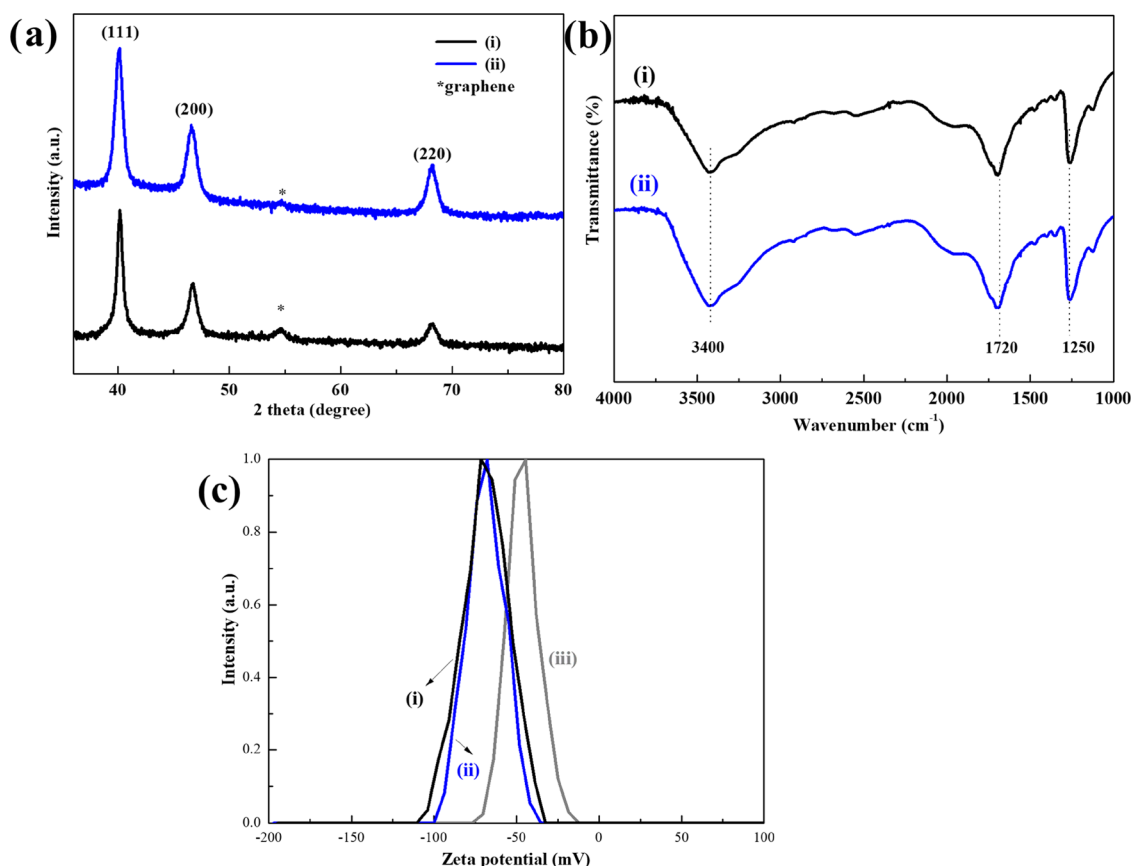


Figure 2. (a) XRD pattern, (b) FT-IR spectra, and (c) ζ -potential of (i) Pd NPs/GR and (ii) sc-Pd NPs/GR composites obtained from oxalic acid at 90 °C, and (iii) graphene.

RESULTS AND DISCUSSION

The as-prepared Pd NPs/GR composites were characterized by TEM, as illustrated in Figure 1. As shown in Figure 1a, the Pd nanoparticles were anchored on the graphene after the PdCl₂ had reacted with the multilayer graphene in the ChCl-oxalic acid DES at 90 °C. Oxalic acid can act as both a solvent and a reducing agent.^{16,32} The TEM images revealed that several particles had become agglomerated. Pd particle growth was due to the strong interactions between the Pd particles and oxygen functional groups on the graphene sheets.¹⁶ The size of the Pd NPs was determined to be around 12.9 ± 2.4 nm. The high-resolution (HR)-TEM image (Figure 1b) indicates that the Pd NP has a cubelike structure. The selected area electron diffraction (SAED) pattern revealed that the Pd cube is polycrystalline.

According to Subramaniam et al.,³³ Pd nanoparticles could be readily and efficiently attached to the surface of graphene sheets using scCO₂ because scCO₂ has no surface tension and exhibits a high wetting ability. With the help of scCO₂, metal or metal oxide nanomaterials with a narrow particle size distribution have been deposited on various carbon supports or inorganic substrates.³⁴ The density of scCO₂ is similar to the liquid-like densities, and metal precursors could be dissolved in scCO₂.³⁵ In addition, compared to other solvents in their liquid form, the mass transfer rates of solute molecules in scCO₂ are considerably faster because scCO₂ possesses a higher penetration rate into porous nanomaterials. Zhao et al. reported on the synthesis of well-dispersed wormlike Pd NPs on pristine graphene (PG) sheets under supercritical CO₂ conditions.³⁶ They found that the scCO₂ had a better surface

wettability for PG and facilitated the deposition of uniform-sized metal Pd species on it, resulting in the generation of a Pd/PG catalyst with an excellent electrical conductivity that could be used in methanol fuel cells. To further understand the effort of an scCO₂ treatment in our system, the as-prepared Pd NPs/GR was treated with scCO₂ by introducing 10.3 MPa of CO₂, and the temperature of the resulting system was maintained at 50 °C for 5 min. The formation of the supercritical fluid-treated Pd NPs/GR (sc-Pd NPs/GR) composite was observed by TEM, as shown in Figure 1d–e. After the scCO₂ treatment, more uniform Pd nanoparticles were dispersed on the surface graphene sheets. The structure of the Pd particles changed to a round shape, and the particle size also decreased to ca. 6.7 ± 1.4 nm. SAED patterns (Figure 1f) indicated that the crystallinity of the material remained the same after the supercritical fluid treatment.

The structure and crystal phase of Pd NPs/GR and sc-Pd NPs/GR composites were characterized by the powder X-ray diffractometer (XRD) to confirm the presence of crystalline Pd nanoparticles in the composites. Figure 2a shows the XRD patterns obtained at $2\theta = 40.1$, 46.3 , and 68.5 , corresponding to the (111), (200), and (220) diffraction of face-centered cubic crystalline geometry of Pd nanoparticle (JCPDS file no. 01-071-3757). The diffraction peak at $2\theta = 54.5$ is related to graphene. These results indicate that the Pd(II) ions can be reduced to form Pd NPs/GR composites by the ChCl-oxalic acid DES because the selected hydrogen-bond donor is an excellent reducing agent for nanoparticle synthesis.³² In the composites, the prominent peaks were assigned to the peaks for Pd nanoparticles. The mean crystallite sizes, D , were

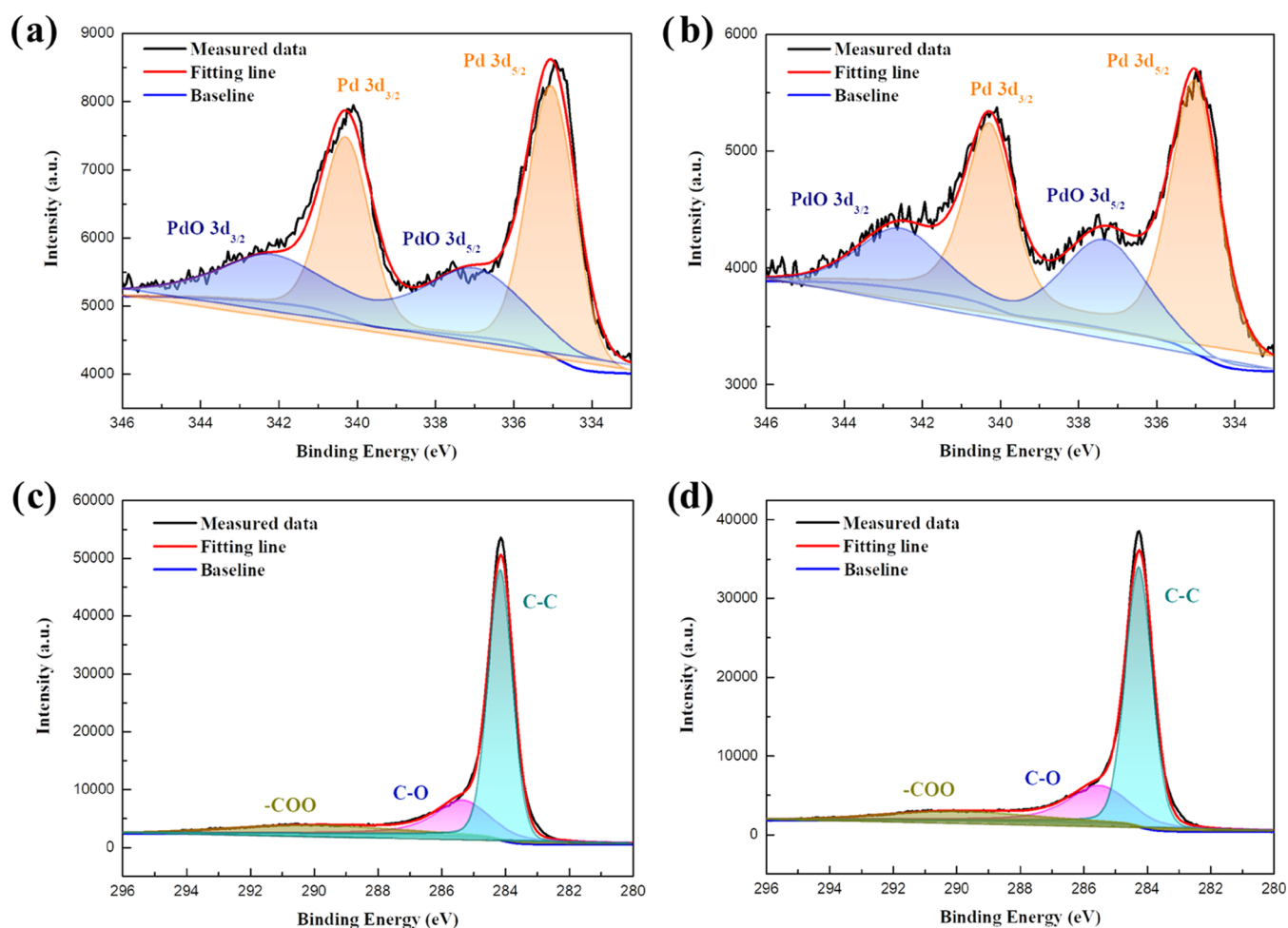


Figure 3. XPS spectra of (a, c) Pd NPs/GR and (b, d) sc-Pd NPs/GR composites obtained from oxalic acid at 90 °C: (a, b) Pd 3d and (c, d) C 1s.

calculated using the Debye–Scherrer formula, $D = K\lambda/(\beta \cos \theta)$, where K is the Scherrer constant, λ is the X-ray wavelength, β is the peak width at half-maximum, and θ is the Bragg diffraction angle. The peak at $2\theta = 40.1$ indicates a calculated crystallite size of 11.06 and 6.98 nm for Pd NPs/GR and sc-Pd NPs/GR, respectively, consistent with the TEM results. Additional structural information regarding the Pd NPs/GR and sc-Pd NPs/GR composites was obtained by Fourier transform infrared (FT-IR) spectroscopy (Figure 2b). The intense broad peak at approximately 3400 cm^{-1} is attributed to the O–H stretching vibration in the spectra. A sharper peak at 1720 cm^{-1} indicates the presence of a free COOH group in the DES. The frequency at 1250 cm^{-1} is related to the C–O stretching frequency. It can be used to recognize the free oxalic acid present in DES.³⁷ These results indicate that, even after the SCF treatment, the oxalic acid remains on the Pd NPs. The ζ -potential provides essential clues concerning the stabilization in the suspension of nanoparticles. A ζ -potential distribution curve of graphene solution (Figure 2c) had a mean value of -44.6 mV . The negative surface charge on the graphene particles resulted from the ionization of hydroxyl groups.³⁸ The zeta potential of Pd NPs/GR was at -71.6 mV , which possessed a more negative value due to the attachment of oxalic acid to the Pd nanoparticles. The ζ -potential of sc-Pd NPs/GR is slightly positively shifted to -67.2 mV because the functional group is slightly reduced by SCF. These zeta potential values are known

to be attributed to the stability of colloids because of the electrostatic repulsion between them.³⁹

The surface composition of the Pd NPs/GR and sc-Pd NPs/GR composites was further characterized by X-ray photoelectron spectroscopy (XPS). Two significant peaks at 335.0 and 340.3 eV in the Pd 3d spectrum of the composites (Figure 3a,b) were assigned to the binding energies of Pd $3d_{5/2}$ and Pd $3d_{3/2}$, respectively, suggesting the presence of metallic Pd. The other two weak peaks at 337.0 and 342.4 eV are ascribed to the presence of PdO.^{40–42} The oxide layer could be due to the surface oxidation of samples during the cleaning and examination. C 1s spectra of the Pd NPs/GR and sc-Pd NPs/GR composites are shown in Figure 3c,d. The prominent C 1s peak at 284.3 eV is contributed by C–C and the other two weak peaks 285.6 and 290.2 eV, corresponding to the C–O bond and the carboxylic group of oxalic acid, respectively.¹⁶ There is no change in XPS data that indicates that the oxalic acid still remains on the Pd NPs/GR composites after the SCF treatment.

ICP-OES emission spectroscopy was used to determine the Pd content in both (sc)-Pd NPs/GR composites. The Pd loading was found to be 14.0 and 16.6 wt % for the Pd NPs/GR and sc-Pd NPs/GR, respectively. The Pd content, as measured by ICP-OES, is consistent with the presence of 15 wt % Pd.

Electrochemical impedance spectroscopy (EIS) was used to examine the kinetics of the electrode reaction and the

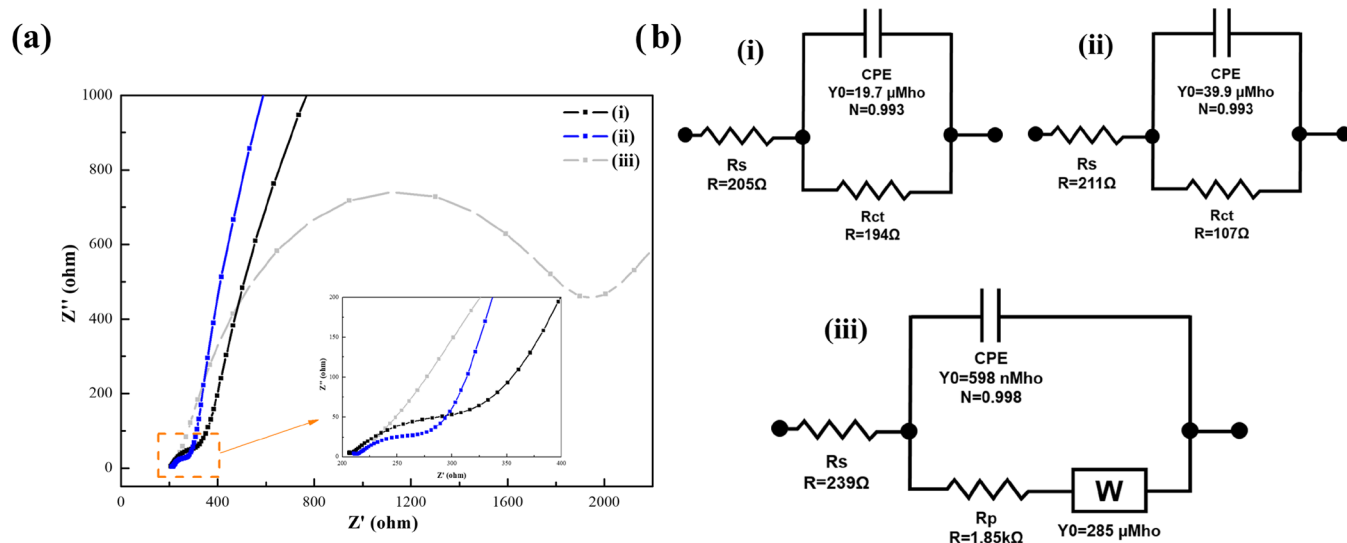


Figure 4. (a) Nyquist plots in 0.1 M KCl containing 5 mM $[\text{Fe}(\text{CN})_6]^{3-/4-}$. (b) Related equivalent circuits for (a): (i) Pd NPs/GR and (ii) sc-Pd NPs/GR composites, and (iii) graphene.

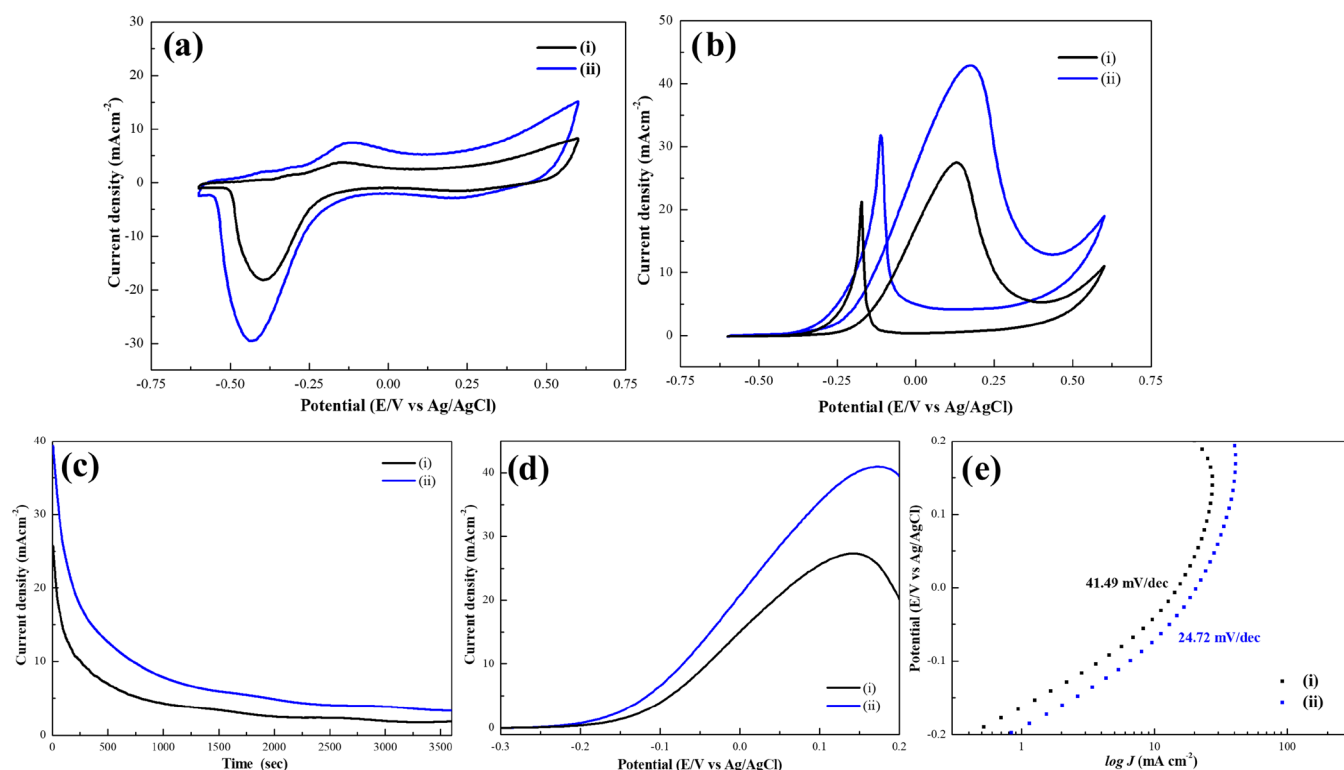


Figure 5. Electrochemical measurement of (i) Pd NPs/GR/SPCE and (ii) sc-Pd NPs/GR/SPCE. (a) CVs recorded in 1 M KOH with a scan rate of 100 mV s^{-1} , (b) CVs recorded in a 1 M glycerol/1 M KOH solution with a scan rate of 50 mV s^{-1} , (c) chronoamperometric stability curves measured at -0.1 V in a 1 M glycerol/1 M KOH solution, (d) linear sweep voltammetry (LSV) curves in a 1 M glycerol/1 M KOH solution with a scan rate of 10 mV s^{-1} , and (e) Tafel plots in a 1 M glycerol/1 M KOH solution.

interfacial process of Pd NPs/GR and sc-Pd NPs/GR composites. The composites were drop-cast on an SPCE as a modified electrode for use in further electrochemical measurements. The Nyquist plots of the EIS include a semicircle, and the diameter of the semicircle is proportional to the charge-transfer resistance (R_{ct}). A smaller diameter indicated that the catalyst had a lower charge-transfer resistance.

Figure 4a shows a Nyquist diagram of the as-prepared modified electrode in a 5 mM $[\text{Fe}(\text{CN})_6]^{3-/4-}/0.1 \text{ M KCl}$

solution. The relative equivalent circuit of these modified electrodes is shown in Figure 4b. While the graphene/SPCE electrode resulted in a sizable semicircle with a high charge-transfer resistance ($R_{ct} = 1850 \Omega$), a decrease in the size of the semicircle and R_{ct} value was observed for the Pd NPs/GR/SPCE (194Ω) and sc-Pd NPs/GR/SPCE (107Ω). This indicates that the catalytic performance of the (sc-) Pd NPs/GR/SPCE is excellent and is due to the rapid electron transfer between the electrode surface and the analyte.

The (sc-) Pd NPs/GR composites were evaluated for their performance toward the electro-oxidation of glycerol as a demonstration of the system. As-prepared Pd modified electrodes were used for the cyclic voltammetry (CV) measurement in 1 M KOH in the absence and presence of 1 M glycerol. Figure 5a shows the CVs for Pd NPs/GR/SPCE and sc-Pd NPs/GR/SPCE in 1 M KOH. Because the Pd atoms on the surface will be oxidized under the given potential, the value for the electrochemically active surface area (ECSA) could be estimated by integrating the reduction charge of the Pd oxide using the reduction charge of $420 \mu\text{C cm}^{-2}$.^{43–45} CV curves of Pd NPs/GR/SPCE and sc-Pd NPs/GR/SPCE show an oxidation wave between +0.25 and +0.6 V that is related to the surface oxidation of Pd. During the reverse scan, a pronounced reduction peak at -0.2 V representing the surface reduction of PdO appeared.⁴⁵ The sc-Pd NPs/GR/SPCE exhibited a much more intense reduction peak than Pd NPs/GR/SPCE, thus revealing that the sc-Pd NPs/GR/SPCE has the largest ECSA. The calculated ECSA values for both modified electrodes were found to be 0.16 and 0.29 cm^2 for Pd NPs/GR and sc-Pd NPs/GR, respectively. The higher ECSA value of the sc-Pd NPs/GR/SPCE may be due to the highly uniform dispersion of Pd nanoparticles on the graphene and the decreased particle size, which was improved by SCF treatment. A comparison between geometrical (0.018 cm^2) and ECSA was conducted to evaluate the effect of combining the Pd NPs and graphene-modified electrodes. When Pd was supported on graphene, the active surface area was increased by 9-fold, and the supercritical fluid treatment improved the distribution of NPs, which also increased the active surface area by 16-fold.

The electrocatalytic performance was further evaluated in a 1 M glycerol/1 M KOH solution, as shown in Figure 5b. Similar to the alcohol oxidation reaction on Pd-based electrocatalysts in alkaline media, the electro-oxidation of glycerol is characterized by the formation of two well-defined anodic current peaks in the forward and reverse scans.^{26,28,45} The freshly chemisorbed species from glycerol adsorption are oxidized in the forward scan. The reverse scan peak is primarily associated with the further electro-oxidation of carbonaceous species, which are not entirely oxidized in the forward scan.^{7,25,31} The appearance of another oxidation peak at a more positive potential at -0.11 V is attributed to the oxidation of the remaining adsorbed OH groups on the catalyst surface and the oxidation of several glycerol products.²⁶ The CVs reveal that the sc-Pd NPs/GR/SPCE has the effect of promoting glycerol oxidation, which shows a more negative onset potential (-0.33 V) and a more significant oxidation current density (42.6 mA cm^{-2}) than the Pd NPs/GR/SPCE (27.3 mA cm^{-2}). Moreover, the sc-Pd NPs/GR/SPCE shifts the current drop toward higher potentials due to the slower kinetics of the formation of the Pd surface oxide on the surface that would delay the surface deactivation by oxide species coverage.⁴⁶ The stabilities and durability of the Pd NPs/GR/SPCE and sc-Pd NPs/GR/SPCE were also evaluated using chronoamperometry at a constant potential of -0.1 V. As shown in Figure 5c, the current densities for all of the catalysts decayed rapidly at the initial stage, implying the formation of intermediate carbonaceous species and poisoning species that were produced during the oxidation of glycerol. The current then gradually deteriorated and eventually reached a pseudo-steady state. As expected, the current density of the sc-Pd NPs/GR/SPCE was higher than that for the Pd NPs/GR/

SPCE over the entire time range. The sc-Pd NPs/GR/SPCE showed the best electrical conductivity, the highest catalytic performance, and showed a higher stability toward GOR. The Tafel slope is a fundamental kinetic parameter associated with a reaction that occurs on the surface of an electrode in an electrochemical reaction. Tafel plots were derived from the linear sweep voltammetry (LSV) data and were used to evaluate the reaction kinetics of electrodes. The LSV curves in Figure 5d show that the sc-Pd NPs/GR/SPCE has the lowest overpotential and highest current density. The catalytic activity is presented in the form of a Tafel plot (Figure 5e), where the logarithm of the current density is plotted against the potential. A lower Tafel slope indicates faster charge-transfer kinetics during the oxidation of glycerol. The calculated Tafel slopes for Pd NPs/GR/SPCE and sc-Pd NPs/GR/SPCE were found to be 41.49 and 27.72 mV/decade, respectively. The slope of the sc-Pd NPs/GR/SPCE possessed a low Tafel slope and remained linear, even at higher current densities, indicating that electron and mass transfer were very rapid during the glycerol oxidation reaction.⁴⁷

CONCLUSIONS

We describe a simple green chemistry approach for preparing carbon-supported Pd electrocatalysts. Pd NPs/GR composites were synthesized in a ChCl–oxalic acid DES by a simple route without the need for any reducing agent or stabilizer. In this process, the DES serves as a reducing agent, a dispersant, and as a solvent during the synthesis process. After treatment with supercritical CO_2 for 5 min, the TEM images indicate that particle sizes and nanoparticle distribution of metal Pd can be adjusted, resulting in the formation of Pd NPs with a narrower particle size distribution on the GR substrate. Interestingly, the sc-Pd NPs/GR/SPCE showed high catalytic activity and long-term stability with respect to the electro-oxidation of glycerol. This approach opens a new area for the synthesis of nanoparticles that contain other metals and alloys using deep eutectic solvents in combination with supercritical fluid techniques.

AUTHOR INFORMATION

Corresponding Authors

Cheng-Kang Chiang – Department of Chemistry, National Dong Hwa University, Hualien City 97401, Taiwan; Phone: +886-3-8903622; Email: ckchiang@gms.ndhu.edu.tw; Fax: +886-3-8900162

Yi-Ting Hsieh – Department of Chemistry, Soochow University, Taipei City 11102, Taiwan; orcid.org/0000-0001-6462-9009; Phone: +886-2-2881-9471; Email: ythsieh@gm.scu.edu.tw; Fax: +886-2-2881-1053

Authors

Cheng-Hao Liao – Department of Chemistry, Soochow University, Taipei City 11102, Taiwan

Jing-Ying Chen – Department of Chemistry, Soochow University, Taipei City 11102, Taiwan

Guang-Yang Liu – Department of Chemistry, National Dong Hwa University, Hualien City 97401, Taiwan

Zhe-Rui Xu – Department of Chemistry, Soochow University, Taipei City 11102, Taiwan

Sheng Lee – Department of Chemistry, Soochow University, Taipei City 11102, Taiwan

Complete contact information is available at:

<https://pubs.acs.org/10.1021/acsomega.2c01721>

Notes

The authors declare no competing financial interest.

ACKNOWLEDGMENTS

This work was supported by the Ministry of Science and Technology, Taiwan of MOST 109-2113-M-259 -007 -MY2 (C.-K.C.) and MOST 109-2113-M-031-001 (Y.-T.H.), MOST 110-2113-M-031-006 (Y.-T.H.), National Dong Hwa University (C.-K.C.), and Soochow University, Taipei, Taiwan (Y.-T.H.). Thanks to C.-Y.C. of the Ministry of Science and Technology (National Taiwan University) for the assistance in the TEM observations.

REFERENCES

- (1) Mehrabi, N.; Lin, H.; Aich, N. Deep eutectic solvent functionalized graphene oxide nanofiltration membranes with superior water permeance and dye desalination performance. *Chem. Eng. J.* **2021**, *412*, No. 128577.
- (2) Abbott, A. P.; Capper, G.; Davies, D. L.; Rasheed, R. K.; Tambyrajah, V. Novel solvent properties of choline chloride/urea mixture. *Chem. Commun.* **2003**, 70–71.
- (3) Smith, E. L.; Abbott, A. P.; Ryder, K. S. Deep Eutectic Solvents (DESs) and Their Applications. *Chem. Rev.* **2014**, *114*, 11060–11082.
- (4) Zhao, B.-Y.; Xu, P.; Yang, F.-X.; Wu, H.; Zong, M.-H.; Lou, W.-Y. Biocompatible Deep Eutectic Solvents Based on Choline Chloride: Characterization and Application to the Extraction of Rutin from *Sophora japonica*. *ACS Sustainable Chem. Eng.* **2015**, *3*, 2746–2755.
- (5) Tomé, L. I. N.; Baião, V.; da Silva, W.; Brett, C. M. A. Deep eutectic solvents for the production and application of new materials. *Appl. Mater. Today* **2018**, *10*, 30–50.
- (6) Hayyan, M.; Abo-Hamad, A.; AlSaadi, M. A.; Hashim, M. A. Functionalization of graphene using deep eutectic solvents. *Nanoscale Res. Lett.* **2015**, *10*, No. 324.
- (7) Atilhan, M.; Costa, L. T.; Aparicio, S. Elucidating the Properties of Graphene–Deep Eutectic Solvents Interface. *Langmuir* **2017**, *33*, 5154–5165.
- (8) Wei, L.; Zhou, Z.-Y.; Chen, S.-P.; Xu, C.-D.; Su, D.; Schuster, M. E.; Sun, S.-G. Electrochemically shape-controlled synthesis in deep eutectic solvents: triambic icosahedral platinum nanocrystals with high-index facets and their enhanced catalytic activity. *Chem. Commun.* **2013**, *49*, 11152–11154.
- (9) Liao, H.-G.; Jiang, Y.-X.; Zhou, Z.-Y.; Chen, S.-P.; Sun, S.-G. Shape-Controlled Synthesis of Gold Nanoparticles in Deep Eutectic Solvents for Studies of Structure–Functionality Relationships in Electrocatalysis. *Angew. Chem., Int. Ed.* **2008**, *47*, 9100–9103.
- (10) Wei, L.; Xu, C.-D.; Huang, L.; Zhou, Z.-Y.; Chen, S.-P.; Sun, S.-G. Electrochemically Shape-Controlled Synthesis of Pd Concave-Disdyakis Triacantahedra in Deep Eutectic Solvent. *J. Phys. Chem. C* **2016**, *120*, 15569–15577.
- (11) Chen, T.; Ying, H.; Zhang, C.; Bi, J.; Li, Z.; Hao, J. Engineering an Fe₂O₃/FeS hybrid catalyst from a deep eutectic solvent for highly efficient electrocatalytic N₂ fixation. *Chem. Commun.* **2021**, *57*, 6688–6691.
- (12) Oh, J.-H.; Lee, J.-S. Synthesis of Gold Microstructures with Surface Nanoroughness Using a Deep Eutectic Solvent for Catalytic and Diagnostic Applications. *J. Nanosci. Nanotechnol.* **2014**, *14*, 3753–3757.
- (13) Lu, L.; An, X. Silver nanoparticles synthesis using H₂ as reducing agent in toluene–supercritical CO₂ microemulsion. *J. Supercrit. Fluids* **2015**, *99*, 29–37.
- (14) Siril, P. F.; Türk, M. Synthesis of Metal Nanostructures Using Supercritical Carbon Dioxide: A Green and Upscalable Process. *Small* **2020**, *16*, No. 2001972.
- (15) Lane, M. K. M.; Zimmerman, J. B. Controlling metal oxide nanoparticle size and shape with supercritical fluid synthesis. *Green Chem.* **2019**, *21*, 3769–3781.
- (16) Tang, L.; Nguyen, V. H.; Shim, J.-J. Supercritical CO₂ mediated synthesis and catalytic activity of graphene/Pd nanocomposites. *Mater. Res. Bull.* **2015**, *71*, 53–60.
- (17) Siril, P. F.; Türk, M. Synthesis of Metal Nanostructures Using Supercritical Carbon Dioxide: A Green and Upscalable Process. *Small* **2020**, *16*, No. 2001972.
- (18) Xie, J.-D.; Wang, C.-H.; Patra, J.; Rath, P. C.; Gandomi, Y. A.; Dong, Q.; Chang, J.-K. Ionic Liquids with Various Constituent Ions To Optimize Non-Enzymatic Electrochemical Detection Properties of Graphene Electrodes. *ACS Sustainable Chem. Eng.* **2019**, *7*, 16233–16240.
- (19) Jiang, D.-H.; Yang, C.-H.; Tseng, C.-M.; Lee, S.-L.; Chang, J.-K. Metal/graphene nanocomposites synthesized with the aid of supercritical fluid for promoting hydrogen release from complex hydrides. *Nanoscale* **2014**, *6*, 12565–12572.
- (20) Chen, C.-Y.; Chang, J.-K.; Tsai, W.-T.; Hung, C.-H. Uniform dispersion of Pd nanoparticles on carbon nanostructures using a supercritical fluid deposition technique and their catalytic performance towards hydrogen spillover. *J. Mater. Chem.* **2011**, *21*, 19063–19068.
- (21) Wu, C.-H.; Wang, C.-H.; Lee, M.-T.; Chang, J.-K. Unique Pd/graphene nanocomposites constructed using supercritical fluid for superior electrochemical sensing performance. *J. Mater. Chem.* **2012**, *22*, 21466–21471.
- (22) Erüinal, E.; Ulusal, F. Thermal effects on hydrogen storage capacity of Pd/MWCNT nanoparticles deposited at moderate pressure and temperature supercritical carbon dioxide conditions. *J. Supercrit. Fluids* **2020**, *157*, No. 104706.
- (23) Erüinal, E.; Ulusal, F.; Aslan, M. Y.; Güzel, B.; Üner, D. Enhancement of hydrogen storage capacity of multi-walled carbon nanotubes with palladium doping prepared through supercritical CO₂ deposition method. *Int. J. Hydrogen Energy* **2018**, *43*, 10755–10764.
- (24) Li, S.; Zhai, Y.; Zhang, X.; MacFarlane, D. R. Surfactant-Free Synthesis of Graphene-Supported PdCu Nanocrystals with High Alloying Degree as Highly Active Catalyst for Formic Acid Electrooxidation. *Adv. Mater. Interfaces* **2017**, *4*, No. 1700227.
- (25) Deng, W.; Chen, J.; Kang, J.; Zhang, Q.; Wang, Y. Carbon nanotube-supported Au-Pd alloy with cooperative effect of metal nanoparticles and organic ketone/quinone groups as a highly efficient catalyst for aerobic oxidation of amines. *Chem. Commun.* **2016**, *52*, 6805–6808.
- (26) Kepenienė, V.; Stagniūnaitė, R.; Bačičūnaitė, A.; Tamašauskaitė-Tamašiūnaitė, L.; Norkus, E. Microwave-assisted synthesis of a AuCeO₂/C catalyst and its application for the oxidation of alcohols in an alkaline medium. *New J. Chem.* **2020**, *44*, 18308–18318.
- (27) Houache, M. S. E.; Hughes, K.; Baranova, E. A. Study on catalyst selection for electrochemical valorization of glycerol. *Sustainable Energy Fuels* **2019**, *3*, 1892–1915.
- (28) Zhao, J.; Jing, W.; Tan, T.; Liu, X.; Kang, Y.; Wang, W. Etching high-Fe-content PtPdFe nanoparticles as efficient catalysts towards glycerol electrooxidation. *New J. Chem.* **2020**, *44*, 4604–4612.
- (29) Sivasakthi, P.; Sangaranarayanan, M. V. Pulse electrodeposited nickel with structure directing agents as an electrocatalyst for oxidation of glycerol. *New J. Chem.* **2019**, *43*, 8352–8362.
- (30) Zakaria, K.; McKay, M.; Thimmappa, R.; Hasan, M.; Mamlouk, M.; Scott, K. Direct Glycerol Fuel Cells: Comparison with Direct Methanol and Ethanol Fuel Cells. *ChemElectroChem* **2019**, *6*, 2578–2585.
- (31) Zhai, C.; Hu, J.; Zhu, M. Three dimensional PdAg nanoflowers as excellent electrocatalysts towards ethylene glycol oxidation. *J. Electroanal. Chem.* **2017**, *806*, 1–7.
- (32) Chowdhury, N. R.; MacGregor-Ramiasa, M.; Zilm, P.; Majewski, P.; Vasilev, K. 'Chocolate' silver nanoparticles: Synthesis, antibacterial activity and cytotoxicity. *J. Colloid Interface Sci.* **2016**, *482*, 151–158.
- (33) Subramaniam, B.; McHugh, M. A. Reactions in supercritical fluids - a review. *Ind. Eng. Chem. Process Des. Dev.* **1986**, *25*, 1–12.

- (34) Sun, Z.; Fan, Q.; Zhang, M.; Liu, S.; Tao, H.; Texter, J. Supercritical Fluid-Facilitated Exfoliation and Processing of 2D Materials. *Adv. Sci.* **2019**, *6*, No. 1901084.
- (35) Barim, S. B.; Uzunlar, E.; Bozbag, S. E.; Erkey, C. Review—Supercritical Deposition: A Powerful Technique for Synthesis of Functional Materials for Electrochemical Energy Conversion and Storage. *J. Electrochem. Soc.* **2020**, *167*, No. 054510.
- (36) Zhao, J.; Liu, Z.; Li, H.; Hu, W.; Zhao, C.; Zhao, P.; Shi, D. Development of a Highly Active Electrocatalyst via Ultrafine Pd Nanoparticles Dispersed on Pristine Graphene. *Langmuir* **2015**, *31*, 2576–2583.
- (37) Saha, S. K.; Dey, S.; Chakraborty, R. Effect of choline chloride-oxalic acid based deep eutectic solvent on the ultrasonic assisted extraction of polyphenols from Aegle marmelos. *J. Mol. Liq.* **2019**, *287*, No. 110956.
- (38) Li, D.; Müller, M. B.; Gilje, S.; Kaner, R. B.; Wallace, G. G. Processable aqueous dispersions of graphene nanosheets. *Nat. Nanotechnol.* **2008**, *3*, 101–105.
- (39) Branko, S.; Dragan, K.; Suzana, F. Measurement and application of zeta-potential. *Rud.-Geol.-Naftni Zb.* **1992**, *4*, No. 147.
- (40) Katayama, Y.; Oshino, Y.; Ichihashi, N.; Tachikawa, N.; Yoshii, K.; Toshima, K. Electrochemical preparation of palladium nanoparticles in bis(trifluoromethylsulfonyl)amide ionic liquids consisting of pyrrolidinium cations with different alkyl chain lengths. *Electrochim. Acta* **2015**, *183*, 37–41.
- (41) Deshmukh, K. M.; Qureshi, Z. S.; Bhatte, K. D.; Venkatesan, K. A.; Srinivasan, T. G.; Rao, P. R. V.; Bhanage, B. M. One-pot electrochemical synthesis of palladium nanoparticles and their application in the Suzuki reaction. *New J. Chem.* **2011**, *35*, 2747–2751.
- (42) Brun, M.; Berthet, A.; Bertolini, J. C. XPS, AES and Auger parameter of Pd and PdO. *J. Electron Spectrosc. Relat. Phenom.* **1999**, *104*, 55–60.
- (43) Arjona, N.; Rivas, S.; Álvarez-Contreras, L.; Guerra-Balcázar, M.; Ledesma-García, J.; Kjeang, E.; Arriaga, L. G. Glycerol electro-oxidation in alkaline media using Pt and Pd catalysts electrodeposited on three-dimensional porous carbon electrodes. *New J. Chem.* **2017**, *41*, 1854–1863.
- (44) Huang, T.-C.; Tsai, H.-C.; Chin, Y.-C.; Huang, W.-S.; Chiu, Y.-C.; Hsu, T.-C.; Chia, Z.-C.; Hung, T.-C.; Huang, C.-C.; Hsieh, Y.-T. Concave Double-Walled AgAuPd Nanocubes for Surface-Enhanced Raman Spectroscopy Detection and Catalysis Applications. *ACS Appl. Nano Mater.* **2021**, *4*, 10103–10115.
- (45) Huang, W.; Kang, X.; Xu, C.; Zhou, J.; Deng, J.; Li, Y.; Cheng, S. 2D PdAg Alloy Nanodendrites for Enhanced Ethanol Electro-oxidation. *Adv. Mater.* **2018**, *30*, No. 1706962.
- (46) Zalineeva, A.; Serov, A.; Padilla, M.; Martinez, U.; Artyushkova, K.; Baranton, S.; Coutanceau, C.; Atanassov, P. B. Self-Supported Pd_xBi Catalysts for the Electrooxidation of Glycerol in Alkaline Media. *J. Am. Chem. Soc.* **2014**, *136*, 3937–3945.
- (47) Yahya, N.; Kamarudin, S. K.; Karim, N. A.; Basri, S.; Zanoodin, A. M. Nanostructured Pd-Based Electrocatalyst and Membrane Electrode Assembly Behavior in a Passive Direct Glycerol Fuel Cell. *Nanoscale Res. Lett.* **2019**, *14*, No. 52.